Theor Chem Acc (2012) 131:1176
DOI 10.1007/s00214-012-1176-0

REGULAR ARTICLE

Toward design of high-performance optoelectronic materials: comparative theoretical studies on the photophysical and charge transport properties of fluorene-based compounds

Guang-Yan Sun · Shui-Xing Wu · Yun Geng · Hai-Bin Li · Yong Wu · Zhong-Min Su

Received: 5 July 2011 / Accepted: 21 December 2011 / Published online: 4 March 2012

Abstract As an important building block for optoelectronic applications, various chemical modifications at C9-position of fluorene have been proposed to enhance its performance by suppressing the well-known keto effect. In order to identify different substitution effects on the photophysical and charge transport properties of fluorene, we systematically study the electronic structures and photophysical behaviors of fluorene (**FR**) and its three dimerized counterparts, namely, 9,9′-spirobifluorene (**SBF**), 9,9′-bifluorenylidene (**BFD**), and bis(biphenyl-2-2-diyl)allene (**BDA**), by employing density functional theory calculations. The changes in bond length alternation indicate that the geometrical relaxations of the fluorene unit in its dimerized derivatives are smaller than **FR** compound. This fact was further proved by the nonradiative decay rate estimated of the first excited singlet state for each compound. Meanwhile, the vibration relaxation analyses suggest that the bridge between two fluorene fragments plays an important role in the nonradiative decay process. In addition, the injection abilities were evaluated in terms of the ionization potentials and electron affinities, and the carrier transport properties were discussed in the framework of Marcus theory. We find **BFD** could be a better ambipolar transport material, and **BDA** can be used as a high-efficient luminescent building unit with excellent hole transport property.

Keywords Fluorene · Dimer · Vibrational relaxation · Electronic spectrum · Density functional theory

1 Introduction

Organic π-conjugated molecules hold considerable attention in optoelectronic applications, such as organic photovoltaic cells (OPVs), dyes sensitized solar cells (DSSCs), and organic light-emitting diodes (OLEDs) [1–6]. It is well known that fluorene has been evolved as an important building block for π-conjugated organic functional materials due to its good thermal stability, high carrier mobility and fluorescence efficiency, wide energy gap in backbones and unique optical and electrochemical properties [7, 8]. Unfortunately, fluorene derivatives such as polyfluorene exhibit a low-energy tailed emission at >500 nm, which has been ascribed to keto effect and/or excimer formation [9, 10] which not only lead to significant decrease in the efficiencies of devices but also results in poor color purity and thus hamper their prospective utilization. Moreover, the high ionization potential (IP) and the low electron affinity (EA) are also unfavorable for hole and electron injection in OLEDs, respectively. As a result, it is of particular importance to make full use of its merits, and at the same time to overcome its deficiency by means of chemical modifications and gain insight into the influence of this modification, toward rational designs for high-performance functional materials.

The keto effect mentioned above results from the easy photo- and/or electro-oxidation at C9-position of fluorene,

Electronic supplementary material The online version of this article (doi:10.1007/s00214-012-1176-0) contains supplementary material, which is available to authorized users.

G.-Y. Sun · Z.-M. Su
Key Laboratory of Natural Resources of Changbai Mountain & Functional Molecules, Ministry of Education, Yanbian University, Yanji 133002, Jilin, China

G.-Y. Sun · S.-X. Wu · Y. Geng · H.-B. Li · Y. Wu · Z.-M. Su (✉)
Institute of Functional Material Chemistry, Faculty of Chemistry, Northeast Normal University, Changchun 130024, Jilin, China
e-mail: zmsu@nenu.edu.cn

leading to the exciton quenching induced by the occurrence of carbonyl group [11–13]. Moreover, the keto defect causes the low-energy tailed emission, which can also be initiated by the formed excimer promoted by keto defect [14–16]. Therefore, to overcome this obstacle, several chemical modifications have been proposed with the aim of taking advantage of the characteristics of fluorene, improving its photophysical properties and adjusting electronic and morphological properties [17–19]. Theoretically, Huang and coworkers [20] have performed a density functional theory (DFT) studies on the structural, electronic and optical properties of the 9-heterofluorenes (replacing *sp*3 carbon with element Si, Ge, N, P, O, S, Se and B). The results demonstrate that it is feasible to improve the ability of carrier injection by tuning frontier orbital energy level of those 9-heterofluorene species. However, such modification cannot overcome the second weakness of 9-heterofluorenes, the tendency of molecular aggregation (vide supra), due to its still planar structure. For this reason, other promising means, especially the two types of dimerization modifications, i.e., the spiro-linkage [21] and the accumulated double bond connection [22] through the C9-position of two fluorene units, evoke our interests. Spiro-linked 9,9′-spirobifluorene (**SBF**) [23, 24] consists of two mutually perpendicular fluorene π systems, which are connected via a common saturated tetracoordinated carbon (spiro-carbon). The spiro-linkage between the two perpendicular oriented π-conjugated segments improves the processibility and the morphologic stability. The rigidity of **SBF** may strengthen the effective π-electron conjugation and suppress nonradiative deactivation pathways, leading to a high photoluminescence quantum yield [25–28]. Thus, **SBF** has been introduced to a wide variety of organic optoelectronic materials, becoming the focus of theoretical and experimental investigations [29–34]. For example, Chiang et al. [35] studied three derivatives of **SBF** theoretically, focusing on the lowest-energy optical transitions. The dynamics and relaxation of photoexcited states of a series of fluorene-containing derivatives were studied by Franco and Tretiak using the excited-state molecular dynamics (ESMD) methodology [36, 37]. They find the spiro-linkage has negligible effect on the emission properties of molecule [38]. As for bis(biphenyl-2-2-diyl)allene (**BDA**) [22], which is composed of two mutually perpendicular fluorene π systems similar to **SBF**, the two fluorene units are connected via a cumulated double bond rather than a saturated C9 atom in **SBF** [39], and the two C9 atoms in **BDA** are embodied in the π-conjugated framework and would have a great influence on the frontier molecular orbitals. 9,9′-bifluorenylidene (**BFD**), another type of dimerization of two fluorene units linked by a direct double bond between the C9 and C9′ atoms, could be also considered as tetrabenzofulvalene. In the ground state, **BFD** presents the twist structure due to the steric interactions between the H1–H1′ and H8–H8′ proton [40–42]. Recently, Brunetti et al. [43] evaluated the potential of this novel family of acceptor compounds based on **BFD** backbone as an alternative to commonly used [6]-phenyl-C_{61}-butyric acid ester ($PC_{60}BM$) in the heterojunction solar cells. Their results showed that the absorption spectra, electronic structures of **BFD** and its derivatives can be effectively tuned upon dimerization with the highest occupied molecular orbital (HOMO) and the lowest unoccupied molecular orbital (LUMO) being in the range of 5.58–5.06 and 3.37–3.09 eV, respectively.

We have analyzed the photophysical properties such as emission energies, second-order nonlinear optical properties and evaluated the ability of charge injection and transport of some fluorene derivative in our previous studies [44, 45]. Here, we carried out comparative DFT and time-dependent (TD) DFT calculations on the electronic structures, spectral and photophysical properties with particular emphasis on fluorescence quantum yields of fluorene-containing derivatives **SBF**, **BFD**, and **BDA** in comparison with **FR** (see Fig. 1) to shed light on the role of this unique chemical modification, dimerization, thus paving the way of designing high-performance optoelectronic materials with good chemical stability. Simultaneously, the injection abilities were also discussed by evaluating the IPs and electron affinities, and the transport properties of holes and electrons were evaluated in the framework of Marcus theory, according to the values of reorganization energies and transfer integrals.

2 Computational methods and theoretical methodology

All calculations were performed with the Gaussian 09 program package [46]. Geometric and electronic structures of the considered fluorene-based compounds were investigated by B3LYP/6-31G(d) [47]. Full geometric optimizations without symmetry constraints were carried out. The geometries of the lowest singlet excited-state (S_1) were optimized with TDDFT [48, 49]. Vibrational frequencies were also evaluated to check that the ground (S_0) and S_1 states were confirmed to be potential energy minima. The transition energies of these fluorene-based compounds were calculated at the optimized ground and excited-state geometries by TDDFT, B3LYP/6-31G(d). The solvent effect of dichloromethane was simulated using the polarizable continuum model (PCM) [50] in which the solvent cavity is regarded as a union of interlocking atomic spheres.

As we know, the fluorescence quantum yield can be expressed as [51]

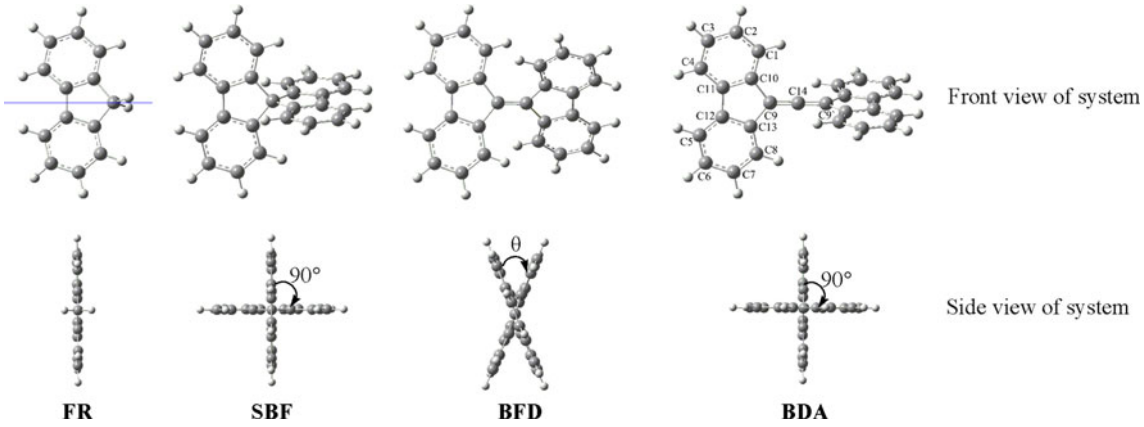

Fig. 1 Chemical structures and bond designations of the investigated systems

$$\eta = k_r/(k_r + k_{nr}) \tag{1}$$

where k_r is the radiative decay rate, k_{nr} is the nonradiative decay rate, including the internal conversion and the intersystem crossing process. k_r can be estimated through the Einstein spontaneous emission relationship, $k_r = f \times E_{if}^2/1.499$, wherein f is the oscillator strength, E_{if} is the excitation energy in cm^{-1}. While intersystem crossing process was not considered in this manuscript because of no heavy atom consisted for all compounds. Thereby, k_{nr} only consists of internal conversion rate k_{ic}.

Under the harmonic approximation, the Born–Oppenheimer internal conversion rate k_{ic} can be given as follows [52–54]:

$$k_{i-f}^{S_1-S_0} = \sum_l \frac{1}{\hbar^2}\left(\frac{\omega_l}{2\hbar}|R_l(fi)|^2\right)\sqrt{\frac{2\pi}{\sum_j S_j\omega_j^2(2\bar{n}_j+1)}} \times \exp\left[-\frac{\left(\omega_{fi}-\omega_l+\sum_j S_j\omega_j\right)^2}{2\sum_j S_j\omega_j^2(2\bar{n}_j+1)}\right] \tag{2}$$

wherein initial state i and final state f mean the lowest excited singlet state and the ground state, respectively. ω_{fi} is the energy difference between the final state and the initial state, and S_j is the Huang–Rhys factor for the jth mode as mentioned above. $\sum_j S_j\omega_j$ represents the sum of relaxation energies for all modes, and $\bar{n}_j$ is the thermally averaged numbers of phonon for jth mode in Boltzman distribution. $R_l(fi) = -\hbar^2\langle\Phi_f|(\partial/\partial Q_l)|\Phi_i\rangle$ is the electronic coupling, which can be given by [55, 56]

$$\left\langle \Phi_f\left|\frac{\partial}{\partial Q_{fl}}\right|\Phi_i\right\rangle = \frac{\left\langle \Phi_f^0\left|\frac{\partial V}{\partial Q_{fl}}\right|\Phi\right\rangle}{E(\Phi_i^0) - E\left(\Phi_f^0\right)} \tag{3}$$

where V denotes the Coulomb interaction potential between the electrons and nuclei, which depends on the position of electrons and nuclei, so

$$\begin{aligned}\left\langle \Phi_f^0\left|\frac{\partial V}{\partial Q_{fl}}\right|\Phi_i^0\right\rangle &= \sum_{\sigma,\alpha} Z_\sigma e^2\left\langle \Phi_f^0\left|\frac{\partial \mathrm{r}_\sigma}{\partial Q_{fl}}\cdot\frac{(\mathrm{r}_\sigma-\mathrm{r}_\alpha)}{|\mathrm{r}_\sigma-\mathrm{r}_\alpha|^3}\Phi_i^0\right|\right\rangle \\ &= \sum_{\sigma,\alpha}\sum_j \frac{Z_\sigma e}{\sqrt{M_\sigma}}\left\langle \Phi_f^0\left|\frac{\partial q_{\sigma j}}{\partial Q_{fl}}\cdot\frac{e(\mathrm{r}_\sigma-\mathrm{r}_\alpha)}{|\mathrm{r}_\sigma-\mathrm{r}_\alpha|^3}\right|\Phi_i^0\right\rangle \\ &= \sum_\sigma \frac{Z_\sigma e}{\sqrt{M_\sigma}}\sum_j E_{f\leftarrow i,\sigma j}L_{f\sigma j,l}\end{aligned} \tag{4}$$

where

$$L_{f\sigma j,l} = \partial q_{\sigma j}/\partial Q_{fl} \tag{5}$$

$$E_{f\leftarrow i,\sigma j} = \left\langle \Phi_f^0\left|E_{\sigma j}\right|\Phi_i^0\right\rangle = \int \mathrm{d}\mathbf{r}\rho_{fi}^0(\mathbf{r})\frac{e(r_{\sigma j}-r_{\alpha j})}{|\mathbf{r}_\sigma-\mathbf{r}_\alpha|^3} \tag{6}$$

$\mathbf{r}_\alpha$ and $\mathbf{r}_\sigma$ are coordinates of the αth electron and the σth nuclei, respectively, and $j = x, y, z$ represents Cartesian components. Z_σ and M_σ represent the number of the nuclear charge and the nuclear mass, respectively. $L_{f\sigma j,l}$ is a component of the lth eigenvector of the Hessian matrix. $E_{f\leftarrow i,\sigma j}$ is the jth component of transition electronic field at atomic center σ, which can be obtained directly from TDDFT calculation. $\rho_{fi}^0(\mathbf{r})$ is the electronic transition density at the equilibrium position, and its contribution to electronic field generated by all electrons at atomic center σ is employed to calculate the $E_{f\leftarrow i,\sigma j}$.

At the microscopic level, the charge transport mechanism can be described as a self-exchange transfer process, in which an electron or hole hops from one charged molecule to an adjacent neutral one. The rate of intermolecular charge transfer (k) can be estimated from semiclassical Marcus theory [57, 58] given in:

$$k = V^2\sqrt{\frac{\pi}{\hbar^2 k_B T\lambda}}\exp\left(-\frac{\lambda}{4k_B T}\right) \tag{7}$$

where V and λ are the transfer integral (also referred to the electronic coupling between adjacent molecules) and the reorganization energy, respectively. $\hbar$ is the Planck

constant, k_B is the Boltzmann constant, and T is the temperature. Therefore, the transfer integral and reorganization energy are two key parameters determining carrier hopping rate. And, we employed the site-energy corrected method [59, 60] (described in supporting information) to evaluate the transfer integral values for all hopping pathways selected from crystal structure of **FR**, **SBF**, **BFD**, and **BDA**. The calculations of transfer integrals were performed at PW91PW91/TZP level, which has been proved to give better estimate of transfer integral. In general, the reorganization energy is cast into contributions from intramolecular vibrations and surrounding medium, namely internal reorganization energy and the external reorganization energy, respectively. Here, the intramolecular reorganization energies of all compounds were evaluated from adiabatic potential energy surfaces at B3LYP/6-311++G(d, p) level, while the external reorganization energies were ignored due to its extremely small contributions to total reorganization energies of the planar conjugation molecules [61, 62].

At a fixed temperature (T), the carrier mobility (μ) can be evaluated from the Einstein relation:

$$\mu = \frac{e}{k_B T} D \tag{8}$$

where e is the electronic charge and D is the diffusion coefficient, which is related to the charge transfer rate k as summing over all possible hops. The diffusion coefficient can be approximately evaluated as [63]:

$$D = \frac{1}{2n} \sum_i r^2 k_i P_i \tag{9}$$

where $n = 3$ is the dimensionality, k_i is the hopping rate due to charge carrier to the ith neighbor, i represents a specific hopping pathway with r being the hopping distance. Here, we assume that the charge hopping occurs only between nearest-neighbor molecules. P_i is the relative probability for charge carrier to a particular ith neighbor:

$$P_i = k_i / \sum_i k_i \tag{10}$$

3 Results and discussion

3.1 Equilibrium geometries between ground state and excited state

The geometric parameters of the optimized structures of **FR** and **BFD** with different density functionals are listed in Table S1. It is obvious that the results given by B3LYP are in good agreement with the experimental values. We also investigated the basis set effect on the optimized geometry of **FR** and the results are listed in Table S2. The results indicate that it is reasonable to optimize these compounds under B3LYP/6-31G(d) level. The monomer of all the compounds selected from the available X-ray crystal diffraction data [45, 65] was optimized by B3LYP/6-31G(d), and the optimized geometries are presented in Table S3 (in Supporting Information). It can be found that the calculated results are in good agreement with the experimental ones except **BDA**. In the crystal, the molecular structure of **BDA** shows a remarkable deviation from linearity (170.1°) of the allene unit [22]. However, the optimized geometry is linear, namely two mutually perpendicular fluorene π systems similar to **SBF**. We speculated that the bend of allene is caused by the packing effects. To prove our assumption, we calculated the geometry of **BDA** based on the crystal structure at the QM/MM level to consider preliminarily the packing effect. The comparison of **BDA** geometry listed in table S4 suggests that the geometry structure calculated by QM/MM model is consistent with the crystal ones. Our predictions proved accurate. Besides, the onion model was also employed to validate the calculation on individual molecule. The comparison of **FR** geometry listed in table S5 suggests that both the geometry structures based on single molecule calculation and onion model are consistent.

As we all know that the extent of the structural deviation between the ground state and the excited state has an important influence on the luminescent efficiency of material, the smaller geometry relaxations, and the smaller nonradiative transition probability. Here, we firstly focus on the degree of geometrical relaxations upon dimerization. The symmetries of **SBF** and **BFD** of excited state are broken due to the non-equivalent geometrical changes of the two fluorene segments. The change of symmetry has been studied by Matuszná et al. [64] for the anionic structures. The optimized geometric parameters of **FR**, **SBF**, **BFD**, and **BDA** in the ground states (S_0) and the lowest singlet excited states (S_1) are presented in Table S3 in Supporting Information at B3LYP/6-31G(d) level. The bond length changes upon excitation for the five-membered ring of fluorene units of **SBF**, **BFD**, and **BDA** are more significant than those in **FR**. The C11–C12, C9–C10, C9–C13 bonds of **SBF**, **BFD**, and **BDA** are shortened, while the neighboring bonds are elongated, which leads to the formation of a quinoide-type structure. Here, we use the bond length alternations (BLA) parameter, which is the difference between the average length of the "single" and "double" bonds, to characterize geometrical changes on individual fluorene fragments. As a structural parameter, BLA has been widely used to interpret electronic spectra of various conjugated molecules [65–68]. The same work also has been calculated by Lukeš et al. [69] for **SBF**. In this work, BLA is defined just for a fluorene unit of molecules:

$$\Delta r_1 = R_{C11-C12} - (R_{C10-C11} + R_{C12-C13})/2 \quad (11)$$

and

$$\Delta r_2 = R_{C11'-C12'} - (R_{C10'-C11'} + R_{C12'-C13'})/2 \quad (12)$$

Table 1 summarizes the BLA values of equilibrium geometries in S_0 and S_1 states and their differences Δr_{e-g}. As seen from Table 1, the Δr_g for the four compounds in S_0 states are similar. In contrast, the Δr_{e1} and Δr_{e2} in S_1 state present remarkable change from **FR** to **BDA**. In addition, the order for Δr_{e-g} is as follows: **FR** > **BFD** > **SBF** > **BDA**, which indicates that the geometrical relaxation of **FR** among the four compounds is the largest, whereas **BDA**'s is the smallest. Since geometrical relaxation from S_0 to S_1 states leading to nonradiative transition, we further infer that the tendency of nonradiative transition rate may conform to **FR** ≈ **BFD** > **SBF** > **BDA**. It should be noted that the Δr_{e-g} just indicates the geometrical relaxation concentrating in five-membered ring of fluorene unit, rather than in twisted angle of the two fluorene units (**BFD** from 34.0° in S_0 to 43.4° in S_1). In what follows, the total geometrical relaxations of these molecules will be further discussed in detail.

3.2 Geometry relaxation and nonradiative decay of the first excited singlet state

TD-B3LYP/6-31G(d) level was employed to optimize the first singlet excited-state geometries of all compounds and to determine their corresponding frequencies. It is generally recognized that Huang–Rhys factor (S_j) characterizing electron-vibration coupling strength is an important physical quantity identifying the extent of the geometry relaxation of excited state [51, 70, 71]. It could be expressed as: $S_j = (\omega_j \Delta Q_j^2)/2\hbar$, where ω_j represents vibration frequency for the jth mode, and ΔQ_j is the normal mode displacement. S_j for each normal mode and the corresponding vibration mode with maximum S_j are shown in Fig. 2. It is found that the largest S_j of **FR** and **SBF** appear in 1,670.9 and 1,662.5 cm^{-1}, respectively, corresponding to the stretching vibrations of C–C double bonds in fluorene fragment. While for **BFD** and **BDA**, their largest Huang–Rhys factors appear in 44.4 and 301.6 cm^{-1}, which are in low frequency region, and the analysis of vibration modes indicates that the former should be the result of C9=C9′ bond twisting and the latter should come from the side—fluorene ring vibrating. For **BDA**, C9=C14=C9′ bonds restrict the stretching vibrations of C–C double bonds in fluorene fragment, and weaker stretching vibrations of C9=C14=C9′ bonds result in weaker extensional stretching vibrations of two sides fluorene units. Among these compounds, **BFD** has the most complex vibration distributions, which suggests that **BFD** may have stronger geometry relaxation of the excited state and thus the largest nonradiative decay in low frequency region, i.e., the vibrations in low frequency region may have important contribution to geometry relaxation due to the weak restriction of C9=C9′. In a word, the different bridges linking two fluorene fragments induce different geometry relaxations of excited state.

Table 1 Calculated values of bond length alternation (in Å) of **FR**, **SBF**, **BFD**, and **BDA** in S_0 and S_1 states

Compounds	FR	SBF	BFD	BDA
Δr_g	0.073	0.073	0.070	0.075
Δr_{e1}	−0.032	0.022	−0.030	0.072
Δr_{e2}	–	0.007	0.004	0.072
Δr_{e1-g}	0.105	0.051	0.100	0.004
Δr_{e2-g}	–	0.066	0.066	0.004

It should be noted that Eq. 2 is applicable to the strong coupling condition, namely $\sum_j S_j \gg 1$. Here, the condition is satisfied basically for these compounds. Meanwhile, low-frequency motions exhibit strong mode mixings, namely Duschinsky rotation effect generally. From table S6, which collects some Duschinsky rotation matrix elements for lowest five frequency modes, we can find that Duschinsky rotation effect is weak for these compounds. Thus, we employed formulas (2–6) to estimate k_{ic} for each compounds and listed the results in Table 2. We can find that **FR** has largest k_{ic}, suggesting that the single fluorene without substituent may have stronger vibration relaxation from the first excited state through C–C stretching vibrations. **SBF** with spiro-linkage has a little smaller k_{ic} than **FR** due to weaker C–C stretching vibrations in high frequency region (about 1,600 cm^{-1}). While the k_{ic} of **BFD** with double bond linkage is 2.32×10^9 s^{-1}, which mainly comes from the contributions of vibrations in low frequency. Specially, **BDA** has an extremely small k_{ic}, 2.75×10^6 s^{-1}, which is considered to be the restriction activity of C9=C14=C9′ bonds. Therefore, **BDA** is speculated to have largest fluorescence quantum yield. In a word, the bridge between the two fluorene fragments plays a decisive role in internal conversion rate, especially for C9=C14=C9′ bonds of **BDA**.

3.3 Frontier molecular orbitals and spectral properties

The frontier molecular orbitals (FMOs) are closely related to the optoelectronic properties such as IP, EA, excitation energy, and charge transportation of the molecules [72]. Here, they are shown in Fig. 3. It is clear that the different types of substitutions at the C-9 position of fluorene bring about different distributions of orbitals and conjugation extent of molecule; thus, the energy levels of **SBF**, **BFD**,

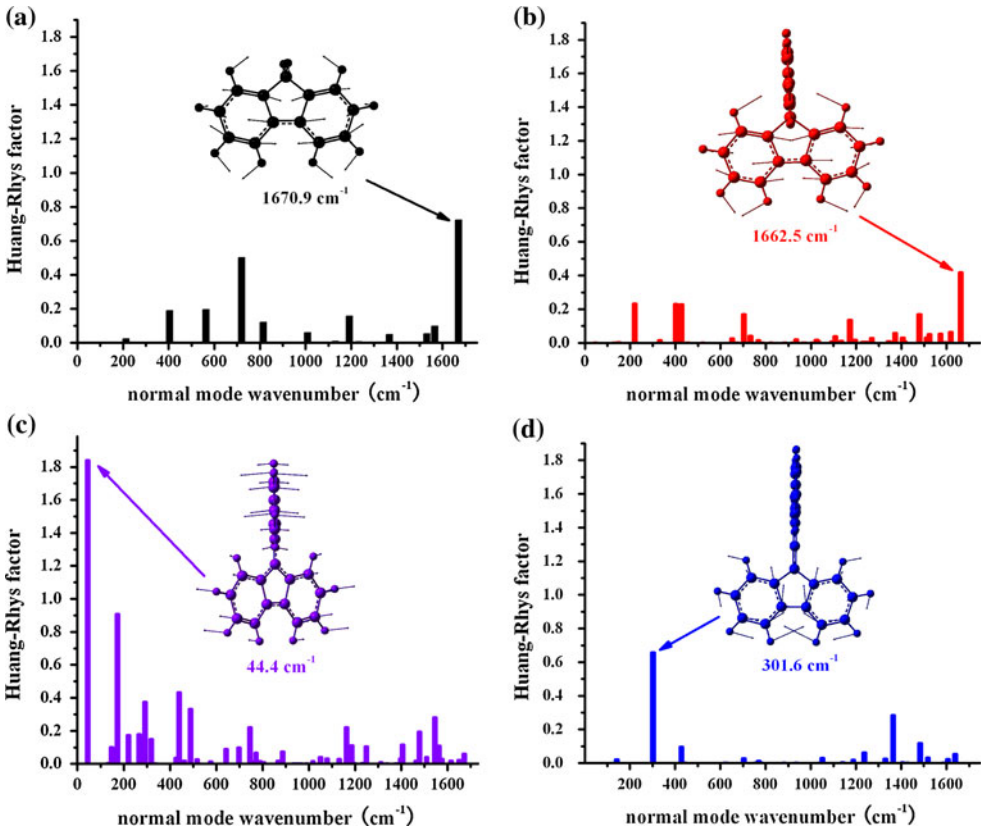

Fig. 2 Calculated Huang–Rhys factors versus the normal mode wave numbers for **FR** (**a**), **SBF** (**b**), **BFD** (**c**), and **BDA** (**d**)

Table 2 The radiative decay rates k_r (s^{-1}) and internal conversion rates k_{ic} (s^{-1}) calculated

Compounds	**FR**	**SBF**	**BFD**	**BDA**
k_r	4.12×10^8	2.84×10^8	9.88×10^7	7.50×10^8
k_{ic}	1.36×10^{10}	5.41×10^9	2.32×10^9	2.75×10^6

and **BDA** are effectively tuned. C9 of **SBF** has little contribution to both the HOMO and LUMO. While for the LUMO, the formation of *spiro*-conjugation between C10 and C1 bond and the adjacent C10′–C1′ bond leads to a slight increase of the delocalized degree in the LUMO. In spite of **BDA** has the larger molecular conjugation by middle double bonds, the C9 of **BDA** also has less contribution to HOMO than **SBF**. The C9 of **BDA** has significant contribution to LUMO, increasing the delocalization of π electron, which results in the decrease of the LUMO energy and make the electronic absorption spectra red-shift. Strikingly, compared to the other compounds, **BFD** is significantly distorted from planarity with a torsional angle of 34.0°. C9 of **BFD** has great contribution to HOMO and LUMO, forming the larger delocalized π-bonds, which results in the increase of the HOMO energy and the decrease of the LUMO energy. These features would results in completely different spectra characteristics.

Absorption and emission energies were calculated at optimized S_0 and S_1 geometries using TD-DFT method to study their optical properties. Simulated Gaussian-type absorption curves of the studied compounds with solvation of dichloromethane (CH_2Cl_2) media are shown in Fig. 4. The detailed information, such as excitation energies, oscillator strengths (f), dominant configurations, transition nature, and experimental values of these compounds, are listed in Table 3. The $S_0 \rightarrow S_1$ electronic transitions for them can be attributed to HOMO to LUMO transition, i.e., π–π^* transition. This indicates that introducing different substitutions at C9-position hardly affects main absorption transition characters of absorption spectra. However, different substitutions have great influences on the oscillator strengths and absorption energies, which are well in agreement with the aforementioned analyses of FMOs. In other word, the bridge between the two fluorene fragments determines the absorption spectrum for these derivatives. The oscillator strength for an electronic transition is proportional to the transition moment reflecting the transition probability between S_0 and S_1. Thus, compared with other compounds, **BFD** may have more intense absorption. In addition, the wavelengths, oscillator strengths, main transition contribution, and the experimental data for emission

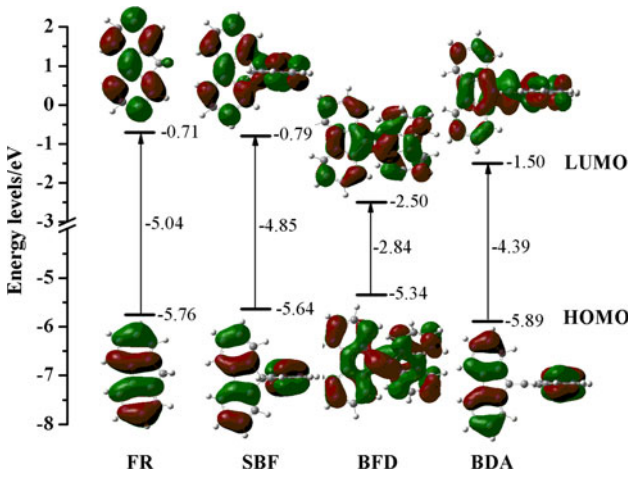

Fig. 3 The FMOs and energy levels of **FR**, **SBF**, **BFD**, and **BDA** at B3LYP/6-31G(d) level

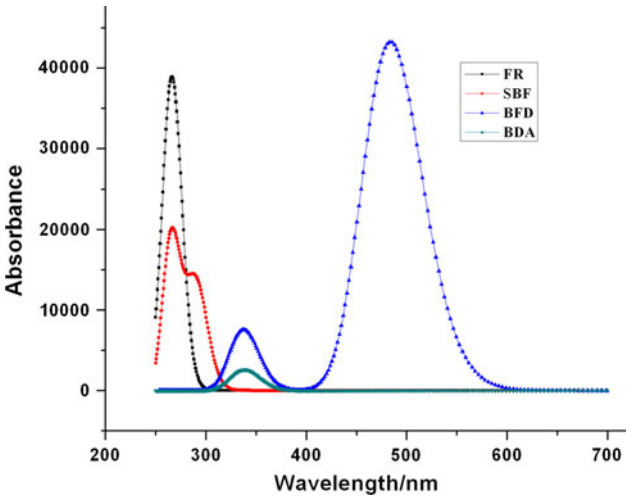

Fig. 4 Simulated absorption spectra in CH_2Cl_2 media for compounds **FR**, **SBF**, **BFD**, and **BDA**. The value of the fwhm is 3,000 cm^{-1}

(λ_{max}) are listed in Table 4. The maximum emission wavelengths of **FR** and **SBF** are 305.4 and 330.9 nm, while the corresponding experimental values are 310 and 325 nm [73], respectively. Thereby, theoretical values agree well with experimental ones, which indicate that the methods we adopted can reflect the variable trend of the emission spectra. Moreover, the calculated Stokes shift of **BFD** (7,567 cm^{-1}) is much larger than those of **FR**, **SBF**, and **BDA**, due to the larger geometrical relaxation around the C9=C9′ double bond.

Based on the emission properties of these compounds, we evaluated all the radiative rates in term of the Einstein spontaneous emission eqn. According to Table 2, the k_r calculated for **FR**, **SBF**, **BFD**, and **BDA** are 4.12×10^8, 2.84×10^8, 9.88×10^7, and 7.50×10^8 s^{-1}, respectively. In experiment, a natural radiative lifetime of 10 ns has been measured for **FR** in CH_2Cl_2, that is, the k_r of **FR** is 1×10^8 s^{-1} [69]. Thus, the evaluations of k_r employing Einstein spontaneous emission relationship are relatively accurate here. Combining with the nonradiative decay rates (internal conversion rates) calculated mentioned above, the fluorescence quantum efficiencies of all compounds were estimated approximately. **FR** and **BDA** were inferred to have lowest and highest fluorescence quantum yields, respectively, among these compounds at single molecule level, and **BDA** may be a potential high-efficient luminescent building unit.

3.4 The charge injection abilities and transport properties

As we know, good charge injection and the comparable transport balance between the holes and electrons are crucial to the high performance of OLEDs [74, 75]. The IP and the EA are usually considered as main parameters in evaluating the ability of charge injection for the different OLED materials [68, 76]. It is well known that the larger EA value of material, the easier an electron from the cathode such as the Al and Ca cross the barrier (ΔE_e) to facilitate electron injection. Likewise, the smaller IP value of material, the easier a hole transfers from the anode (ITO) to the adjacent hole transport layer in OLEDs. Furthermore, reorganization energy (λ) should be taken into account to assess the degree of geometrical relaxation of molecule in the process of charge transport. Note that the smaller value of the reorganization energy means the stronger rigidity of molecule and further the easier charge transport [77, 78]. The values of EA, IP, and λ estimated are listed in Table 5. It should be noted that although B3LYP/6-31G(d) give enough accurate estimate of geometric and electronic structures for all compounds, B3LYP/6-31++G(d, p) were also employed to calculate the EA/IP and λ to obtain more accurate values according to the comparisons in table S7–S8. Firstly, according to Table 5, the values of IP of **SBF**, **BFD**, and **BDA** show a significant decrease, while the values of EA show a significant increase, compared with **FR**. Especially for **BFD**, it possesses the largest EA and the smallest IP values, which suggests that **BFD** may show excellent performance in charge injection. The trends are in agreement with those of HOMOs and LUMOs. Secondly, the results in Table 5 also show that the differences between λ_{ie} and λ_{ih} ($\Delta\lambda_{e/h}$) for **FR** (0.011 eV), **SBF** (0.042 eV), and **BFD** (0.051 eV) are small. Combining with the analysis of EA and IP, we conclude that the small $\Delta\lambda_{e/h}$ of **BFD** facilitates charge transfer balance and the formation of the exciton. While very low values of EA for **FR** and **SBF** are not favorable for electron injection from the cathode. However, for **BDA**, the unbalanced values between λ_{ih} (0.124 eV) and λ_{ie} (1.166 eV) determine that **BDA** could be just used as an

Table 3 Selected excitation energies (eV), wavelengths (nm), oscillator strengths (*f*) for low-lying singlet excited states of **FR**, **SBF**, **BFD**, and **BDA** calculated in CH_2Cl_2 at TD-B3LYP/6-31G(d, p) level

Compounds	Cal. (nm)	Composition	*f*	$\lambda_{exp.}$
FR	267.8	H → L (0.77)	0.4445	265[a]
		H → L + 1 (0.12)		
SBF	290.6	H → L (0.91)	0.0910	297[a]
	265.7	H-1 → L (0.81)	0.2594	252[a]
	265.7	H-1 → L + 1 (0.81)	0.2594	252[a]
	231.8	H-1 → L + 3 (0.54)	0.3738	229[a]
BFD	463	H → L (0.71)	1.0000	458[b]
BDA	341.3	H → L (0.27)	0.0000	
		H-2 → L + 1 (0.47)		
	310.9	H-3 → L (0.45)	1.2386	
		H-2 → L + 1 (0.45)		

H HOMO, *L* LUMO

[a] Experimental data from Ref. [73]

[b] Experimental data from Ref. [43]

Table 4 Selected emission energies (eV), emission wavelengths (nm), and oscillator strengths (*f*) for low-lying singlet excited states of **FR**, **SBF**, **BFD**, and **BDA** calculated in CH_2Cl_2

Compounds	Cal. (nm/eV)	Composition	*f*	$\lambda_{exp.}$[a] (nm)
FR	305.4/4.06	L → H (0.98)	0.5767	310.0
		L + 1 → H (0.12)		
SBF	330.9/3.75	L → H (0.93)	0.0649	325.0
	292.6/4.24	L → H-1 (0.89)	0.3643	
BFD	712.7/1.74	L → H-1 (1.00)	0.0012	
	604.4/2.05	L → H (1.00)	0.5413	
BDA	373.1/3.32	L → H-3 (0.49)	0.0000	
		L + 1 → H-2 (0.49)		
	332.8/3.73	L + 1 → H-2 (0.49)	1.2459	
		L → H-3 (0.49)		

H HOMO, *L* LUMO

[a] Experimental data from Ref. [73]

Table 5 IP, EA, internal reorganization energy of hole (λ_{ih}) and electron (λ_{ie}) by B3LYP/6-311++G(d, p) calculation (in eV), and the hole (μ_h) and electron mobilities (μ_e) (in cm^2/V s)

Compounds	IP_v	IP_a	EA_v	EA_a	λ_{ih}	λ_{ie}	μ_h	μ_e
FR	7.762	7.631	−0.373	−0.242	0.261	0.272	7.61×10^{-2}	1.49×10^{-1}
SBF	7.298	7.228	0.003	0.094	0.139	0.181	2.48×10^{-1}	4.81×10^{-2}
BFD	6.956	6.808	1.631	1.808	0.303	0.354	4.72×10^{-2}	6.09×10^{-2}
BDA	7.441	7.378	0.712	1.147	0.124	1.166	4.60	6.30×10^{-6}
9,9-dimethyl-9*H*-fluorene	7.682[a]	7.548	−0.301	−0.168	0.269	0.272	–	–

[a] The experimental values of IP in Ref. [79] is 7.850 eV for 9,9-dimethyl-9*H*-fluorene

excellent hole transport material. It should be noted that the λ is just one of the key factors that influence the electron and hole mobilities of compounds, and other factors like electronic coupling (electron and hole transfer integral) are not taken into account.

To obtain rational transfer integrals (*V*), all of the possible hopping pathways (dimer) of all compounds have been considered based on their crystal structures. The hopping pathways of compounds are shown in Figure S2–S5 of Supporting Information. Their corresponding dimer center of mass (CM) distances and transfer integrals are also presented in Table S9–S12. In what follows, the hole and electron mobilities of **FR** (7.61×10^{-2} and 1.49×10^{-1} cm^2/V s), **SBF** (2.48×10^{-1} and 4.81×10^{-2} cm^2/V s), **BFD** (4.72×10^{-2} and 6.09×10^{-2} cm^2/V s), and **BDA** (4.60 and 6.30×10^{-6} cm^2/V s) were estimated, respectively, according to the values of reorganization energies and transfer integrals in the framework of Marcus theory, which further prove the above-mentioned discussion, i.e., **SBF** and **BDA** may present large intrinsic hole mobility, and **BFD** may be a good ambipolar transport material.

4 Conclusions

In the manuscript, systematical computational investigations were performed on the fluorene and its derivatives **SBF**, **BFD,** and **BDA** to gain better understanding about

the influences of dimerization on the photophysical and charge transport properties. The analyses of geometrical features at ground and excited states through BLA calculation give a preliminary explanation of the influence of the bridge between the two fluorene fragments. Then, the discussion on the vibrational relaxations and the internal conversion rates of the first singlet excited states indicate that the cumulated double bond of **BDA** can restrict the relaxation of excited state and thus improve the luminescence quantum efficiency, and the following fluorescence quantum yields estimated further suggest **BDA** may be a potential high-efficient luminescent building unit. It is also find that the absorption/emission spectra characteristics are completely different, which is ascribed to the different FMOs induced by different bridges at C9-linked. Meanwhile, the transport properties were discussed in the framework of Marcus theory, according to the values of reorganization energies and transfer integrals. Our calculations demonstrate that **SBF** may present large intrinsic hole mobility, while **BFD** may be a good ambipolar transport material, and **BDA** may present large intrinsic hole mobility. In a word, these discussions on photophysical and charge transport properties of these fluorene dimer derivatives indicate the bridge play a decisive role.

Acknowledgments We gratefully acknowledge the financial support from the National Natural Science Foundation of China (Project No. 20903020), National Basic Research Program of China (973 Program-2009CB623605), the Science and Technology Development Project Foundation of Jilin Province (20090146), the Science and Technology Development Planning of Yan Bian University (201103).

References

1. Lu Y, Zhou Y, Quan YW, Chen QM, Chen RF, Zhang ZY, Fan QL, Huang W, Ding JF (2011) Org Lett 13:200. doi:10.1021/ol1025958
2. Sorensen JK, Fock J, Pedersen AH, Petersen AB, Jennum K, Bechgaard K, Kilsa K, Geskin V, Cornil J, Bjornholm T, Nielsen MB (2011) J Org Chem 76:245. doi:10.1021/jo102066x
3. Yildirim M, Kaya I (2011) Synth Met 161:13. doi:10.1016/j.synthmet.2010.10.028
4. Yu DH, Zhao YBA, Xu H, Han CM, Ma DG, Deng ZP, Gao S, Yan PF (2011) Chem Eur J 17:2592. doi:10.1002/chem.201003434
5. Zafra JL, Casado J, Perepichka II, Perepichka IF, Bryce MR, Ramirez FJ, Navarrete JTL (2011) J Chem Phys 134:044520. doi:10.1063/1.3526487
6. Zhong HL, Lai H, Fang QA (2011) J Phys Chem C 115:2423. doi:10.1021/jp109806m
7. Tao Y, Yang C, Qin J (2011) Chem Soc Rev 40:2943. doi:10.1039/C0CS00160K
8. Burns DM, Iball J (1955) Proc R Soc Lond A 227:200. doi:10.1098/rspa.1955.0004
9. Zeng G, Yu WL, Chua SJ, Huang W (2002) Macromolecules 35:6907. doi:10.1021/ma020241m
10. Chen XW, Tseng HE, Liao JL, Chen SA (2005) J Phys Chem B 109:17496. doi:10.1021/jp052549w
11. Gadermaier C, Romaner L, Piok T, List EJW, Souharce B, Scherf U, Cerullo G, Lanzani G (2005) Phys Rev B 72:1. doi:10.1103/PhysRevB.72.045208
12. Hayer A, Khan ALT, Friend RH, Kohler A (2005) Phys Rev B 71:1. doi:10.1103/PhysRevB.71.241302
13. Abad S, Bosca F, Domingo LR, Gil S, Pischel U, Miranda MA (2007) J Am Chem Soc 129:7407. doi:10.1021/ja0712827
14. Kuik M, Wetzelaer GJAH, Laddé JG, Nicolai HT, Wildeman J, Sweelssen J, Blom PWM (2011) Adv Funct Mater 21:4502. doi:10.1002/adfm.201100374
15. Kulkarni AP, Kong XX, Jenekhe SA (2004) J Phys Chem B 108:8689. doi:10.1021/jp037131h
16. Vacha M, Ha J, Ito Y, Shimada T, Mo SJ, Sato H (2005) Appl Phys Lett 97:023514. doi:10.1063/1.1831542
17. Greczynski G, Fahlman M, Salaneck WR (2000) Chem Phys Lett 321:379. doi:10.1016/S0009-2614(00)00338-9
18. Klaerner G, Miller RD (1998) Macromolecules 31:2007. doi:10.1021/ma971073e
19. Wong KT, Chien YY, Chen RT, Wang CF, Lin YT, Chiang HH, Hsieh PY, Wu CC, Chou CH, Su YO, Lee GH, Peng SM (2002) J Am Chem Soc 124:11576. doi:10.1021/ja0269587
20. Chen RF, Zheng C, Fan QL, Huang W (2007) J Comput Chem 28:2091. doi:10.1002/jcc.20591
21. Clarkson RG, Gomberg M (1930) J Am Chem Soc 52:2881. doi:10.1021/ja01370a048
22. Fenimore CP (1948) Acta Crystallogr 1:295. doi:10.1107/s0365110x4800082x
23. Douthwaite RE, Taylor A, Whitwood AC (2005) Acta Crystallogr Sect C: Cryst Struct Commun 61:o328. doi:10.1107/s0108270105009479
24. Schenk H (1972) Acta Crystallogr Sect B: Struct Sci 28:625. doi:10.1107/s0567740872002869
25. Zhao C-H, Wakamiya A, Inukai Y, Yamaguchi S (2006) J Am Chem Soc 128:15934. doi:10.1021/ja0637550
26. Wakamiya A, Ide T, Yamaguchi S (2005) J Am Chem Soc 127:14859. doi:10.1021/ja0537171
27. Wakamiya A, Mishima K, Ekawa K, Yamaguchi S (2008) Chem Comm 579. doi:10.1039/b716107g
28. VandenBout DA, Yip WT, Hu DH, Fu DK, Swager TM, Barbara PF (1997) Science 277:1074. doi:10.1126/science.277.5329.1074
29. Yan M, Rothberg LJ, Kwock EW, Miller TM (1995) Phys Rev Lett 75:1992. doi:10.1103/PhysRevLett.75.1992
30. Huser T, Yan M, Rothberg LJ (2000) Proc Natl Acad Sci USA 97:11187. doi:10.1073/pnas.97.21.11187
31. Schwartz BJ (2003) Annu Rev Phys Chem 54:141. doi:10.1146/annurev.physchem.54.011002.103811
32. Nguyen TQ, Wu JJ, Doan V, Schwartz BJ, Tolbert SH (2000) Science 288:652. doi:10.1126/science.288.5466.652
33. Kim J, Swager TM (2001) Nature 411:1030. doi:10.1038/35082528
34. Hu DH, Yu J, Wong K, Bagchi B, Rossky PJ, Barbara PF (2000) Nature 405:1030. doi:10.1038/35016520
35. Chiang CL, Shu CF (2002) Chem Mater 14:682. doi:10.1021/cm010665f
36. Franco I, Tretiak S (2004) J Am Chem Soc 126:12130. doi:10.1021/ja0489285
37. Franco I, Tretiak S (2003) Chem Phys Lett 372:403. doi:10.1016/S0009-2614(03)00419-6
38. Culligan SW, Geng YH, Chen SH, Klubek K, Vaeth KM, Tang CW (2003) Adv Mater 15:1176. doi:10.1002/adma.200304972
39. Weber E, Seichter W, Hess B, Will G, Dasting HJ (1995) J Phys Org Chem 8:94. doi:10.1002/poc.610080207
40. Lee JS, Nyburg SC (1985) Acta Crystallogr Sect C: Cryst Struct Commun 41:560. doi:10.1107/S010827018500467X
41. Pogodin S, Agranat I (2002) J Org Chem 67:265. doi:10.1021/jo0107251

42. Riklin M, von Zelewsky A, Bashall A, McPartlin M, Baysal A, Connor JA, Wallis JD (1999) Helv Chim Acta 82:1666. doi:10.1002/(SICI)1522-2675(19991006)82:10<1666:AID-HLCA1666>3.0.CO;2-K
43. Brunetti FG, Gong X, Tong M, Heeger AJ, Wudl F (2010) Angew Chem Int Ed 49:532. doi:10.1002/anie.200905117
44. Yang SY, Kan YH, Yang GC, Su ZM, Zhao L (2006) Chem Phys Lett 429:180. doi:10.1016/j.cplett.2006.07.078
45. Yang GC, Su ZM, Qin CS (2006) J Phys Chem A 110:4817. doi:10.1021/jp0600099
46. Frisch M, Trucks GW, Schlegel HB, Scuseria GE, Robb MA, Cheeseman JR, Scalmani G, Barone V, Mennucci BG, Petersson A, Nakatsuji H, Caricato M, Li X, Hratchian HP, Izmaylov AF, Bloino J, Zheng G, Sonnenberg JL, Hada M, Ehara M, Toyota K, Fukuda R, Hasegawa J, Ishida M, Nakajima T, Honda Y, Kitao O, Nakai H, Vreven T, Montgomery JA Jr, Peralta JE, Ogliaro F, Bearpark M, Heyd JJ, Brothers E, Kudin KN, Staroverov VN, Kobayashi R, Normand J, Raghavachari K, Rendell A, Burant JC, Iyengar SS, Tomasi J, Cossi M, Rega N, Millam JM, Klene M, Knox JE, Cross JB, Bakken V, Adamo C, Jaramillo J, Gomperts R, Stratmann RE, Yazyev O, Austin AJ, Cammi R, Pomelli C, Ochterski JW, Martin RL, Morokuma K, Zakrzewski VG, Voth GA, Salvador P, Dannenberg JJ, Dapprich S, Daniels AD, Farkas O, Foresman JB, Ortiz JV, Cioslowski J, Fox DJ (2009) Gaussian 09, revision A.02. Gaussian, Wallingford
47. Lee CT, Yang WT, Parr RG (1988) Phys Rev B 37:785. doi:10.1103/PhysRevB.37.785
48. Casida ME, Jamorski C, Casida KC, Salahub DR (1998) J Chem Phys 108:4439. doi:10.1063/1.475855
49. Stratmann RE, Scuseria GE, Frisch MJ (1998) J Chem Phys 109:8218. doi:10.1063/1.477483
50. Tomasi J, Mennucci B, Cammi R (2005) Chem Rev 105:2999. doi:10.1021/cr9904009
51. Peng Q, Yi Y, Shuai Z, Shao J (2007) J Am Chem Soc 129:9333. doi:10.1021/ja067946e
52. Lin SH, Bersohn R (1965) J Chem Phys 44:3768. doi:10.1063/1.1726532
53. Lin SH (1965) J Chem Phys 44:3759. doi:10.1063/1.1726531
54. Lin SH, Chang CH, Liang KK, Chang R, Shiu YJ, Zhang JM, Yang TS, Hayashi M, Hsu FC (2002) Adv Chem Phys 121:1. doi:10.1002/0471264318.ch1
55. Hayashi M, Mebel AM, Liang KK, Lin SH (1998) J Chem Phys 108:2044. doi:10.1063/1.475584
56. Niu Y, Peng Q, Deng C, Gao X, Shuai Z (2010) J Phys Chem A 114:7817. doi:10.1021/jp101568f
57. Marcus RA (1993) Rev Mod Phys 65:599. doi:10.1103/RevModPhys.65.599
58. Marcus RA, Sutin N (1985) Biochim Biophys Acta Bioenerg 811:265. doi:10.1016/0304-4173(85)90014-X
59. Valeev EF, Coropceanu V, da Silva DA, Salman S, Bredas JL (2006) J Am Chem Soc 128:9882. doi:10.1021/ja061827h
60. Geng Y, Li HB, Wu SX, Duan YA, Su ZM, Liao Y (2011) Theor Chem Acc 129:247. doi:10.1007/s00214-011-0928-6
61. McMahon DP, Troisi A (2010) J Phys Chem Lett 1:941. doi:10.1021/jz1001049
62. Norton JE, Bredas JL (2008) J Am Chem Soc 130:12377. doi:10.1021/ja8017797
63. Yang XD, Wang LJ, Wang CL, Long W, Shuai ZG (2008) Chem Mater 20:3205. doi:10.1021/cm8002172
64. Matuszná K, Breza M, Pálszegi T (2008) J Mol Struct Theochem 851:277. doi:10.1016/j.theochem.2007.11.020
65. Kan YH, Yang GC, Yang SY, Zhang M, Lan YQ, Su ZM (2006) Chem Phys Lett 418:302. doi:10.1016/j.cplett.2005.11.005
66. Marder SR, Perry JW, Bourhill G, Gorman CB, Tiemann BG, Mansour K (1993) Science 261:186. doi:10.1126/science.261.5118.186
67. Ohira S, Hales JM, Thorley KJ, Anderson HL, Perry JW, Bredas JL (2009) J Am Chem Soc 131:6099. doi:10.1021/ja9007003
68. Shi LL, Liao Y, Yang GC, Su ZM, Zhao SS (2008) Inorg Chem 47:2347. doi:10.1021/ic7018154
69. Lukeš V, Šolc R, Milota F, Sperling J, Kauffmann HF (2008) Chem Phys 349:226. doi:10.1016/j.chemphys.2008.02.066
70. Geng Y, Wu SX, Li HB, Tang XD, Wu Y, Su ZM, Liao Y (2011) J Mater Chem 21:15558. doi:10.1039/c1jm12483h
71. Yin SW, Peng Q, Shuai Z, Fang WHY, Wang YH, Luo Y (2006) Phys Rev B 73:205409. doi:10.1103/PhysRevB.73.205409
72. Liao Y, Yang GC, Feng JK, Shi LL, Yang SY, Yang L, Ren AM (2006) J Phys Chem A 110:13036. doi:10.1021/jp061326i
73. Horhant D, Liang JJ, Virboul M, Poriel C, Alcaraz G, Rault-Berthelot J (2006) Org Lett 8:257. doi:10.1021/ol0526064
74. Shirota Y, Kageyama H (2007) Chem Rev 107:953. doi:10.1021/cr050143+
75. Kulkarni AP, Tonzola CJ, Babel A, Jenekhe SA (2004) Chem Mater 16:4556. doi:10.1021/cm049473l
76. Li XN, Wu ZJ, Si ZJ, Zhang HJ, Zhou L, Liu XJ (2009) Inorg Chem 48:7740. doi:10.1021/ic900585p
77. Geng Y, Wang JP, Wu SX, Li HB, Yu F, Yang GC, Gao HZ, Su ZM (2011) J Mater Chem 21:134. doi:10.1039/c0jm02119a
78. Tang XD, Gao HZ, Geng Y, Liao Y, Su ZM (2010) Chem J Chin Univ 31:766
79. Rathore R, Abdelwahed SH, Guzei IA (2003) J Am Chem Soc 125:8712. doi:10.1021/ja035518s